The characterisation of diesel exhaust particles - composition, size distribution and partitioning

Alam, Mohammed S; Zeraati-Rezaei, Soheil; Stark, Christopher P; Liang, Zhirong; Xu, Hongming; Harrison, Roy M

DOI:
10.1039/C5FD00185D
10.1039/c5fd00185d

Faraday Discussions

Accepted Manuscript

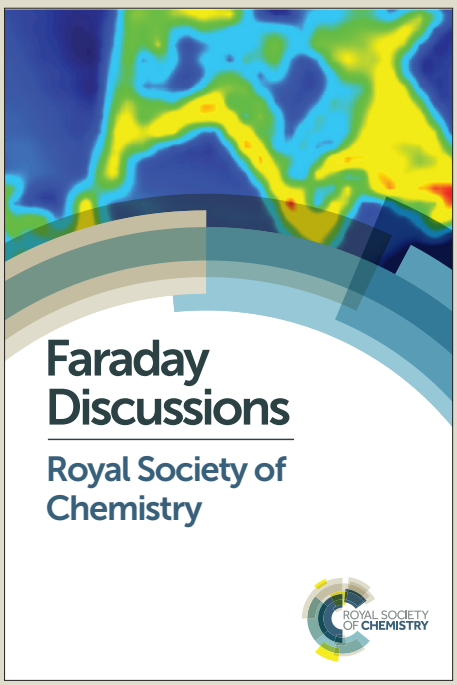

This article can be cited before page numbers have been issued, to do this please use: M. S. Alam, S. Zeraati-Rezaei, C. Stark, Z. Liang, H. Xu and R. M. Harrison, *Faraday Discuss.*, 2016, DOI: 10.1039/C5FD00185D.

View Article Online
DOI: 10.1039/C5FD00185D

The characterisation of diesel exhaust particles – composition, size distribution and partitioning

Mohammed S. Alam[1], Soheil Zeraati-Rezaei[2], Christopher P. Stark[1], Zhirong Liang[2], Hongming Xu[2] and Roy M. Harrison[1*†]

[1] Division of Environmental Health and Risk Management
School of Geography, Earth and Environmental Sciences
University of Birmingham
Edgbaston, Birmingham B15 2TT
United Kingdom

[2] School of Mechanical Engineering
University of Birmingham
Edgbaston, Birmingham B15 2TT
United Kingdom

* To whom correspondence should be addressed.
Tele: +44 121 414 3494; Fax: +44 121 414 3708; Email: r.m.harrison@bham.ac.uk

†Also at: Department of Environmental Sciences / Center of Excellence in Environmental Studies, King Abdulaziz University, PO Box 80203, Jeddah, 21589, Saudi Arabia

DOI: 10.1039/C5FD00185D

Abstract

A number of major research questions remain concerning the sources and properties of road traffic generated particulate matter. A full understanding of the composition of primary vehicle exhaust aerosol and its contribution to secondary organic aerosol (SOA) formation still remains elusive, and many uncertainties exist relating to the semi-volatile component of the particles. Semi-Volatile Organic Compounds (SVOC) are compounds which partition directly between the gas and aerosol phases under ambient conditions. The SVOC in engine exhaust are typically hydrocarbons in the C_{15}-C_{35} range, and are largely uncharacterised because they are unresolved by traditional gas chromatography and form a large hump in the chromatogram referred to as Unresolved Complex Mixture (UCM).

In this study, thermal desorption coupled to comprehensive two dimensional Gas-Chromatography Time-of-Flight Mass-Spectrometry (TD-GC×GC-ToF-MS) was exploited to characterise and quantify the composition of SVOC from the exhaust emission. Samples were collected from the exhaust of a diesel engine, sampling before and after a diesel oxidation catalyst (DOC), while testing at steady state conditions. Engine exhaust was diluted with air and collected using both filter and impaction (nano-MOUDI), to resolve total mass and size resolved mass respectively. Adsorption tubes were utilised to collect SVOC in the gas phase and analysed using thermal desorption, while particle size distribution was evaluated by sampling with a DMS500.

The SVOC was observed to contain predominantly *n*-alkanes, branched alkanes, alkyl-cycloalkanes, alkyl-benzenes, PAH and various cyclic aromatics. Particle phase compounds identified were similar to those observed in engine lubricants, while vapour phase constituents were similar to those measured in fuels. Preliminary results are presented illustrating differences in the particle size distribution and SVOC composition when collecting samples with and without a DOC. The results indicate that the DOC tested is of very limited efficiency, under the studied engine operating conditions, for removal of SVOC, especially at the upper end of the molecular weight range.

DOI: 10.1039/C5FD00185D

1.0 Introduction

Urban air pollution is comprised of a highly complex mixture of compounds both in the vapour and particulate phase. These complex mixtures can enter the atmosphere through various natural and anthropogenic processes such as incomplete combustion of fossil fuels, biomass burning and forest fires and may also be formed as products of gas to particle conversion through atmospheric reactions. Urban areas therefore, provide a natural focus for research on air quality as they experience high emissions from space heating and road transport associated with their high population densities.[1] Road traffic generated particulate matter (PM) has gained major interest over the last few decades owing to their associated detrimental impacts on human health.[2-4] PM emissions from road vehicles can be generated from exhaust and non-exhaust emission types; for example, exhaust tailpipe and abrasion of vehicle parts including brakes, clutch and tyres, and re-suspension of dust.[5] There are currently more than 37 million vehicles on UK roads. In 1994 the UK diesel passenger cars comprised 7.4% of the fleet and increased to 34.5% of the total by 2013.[6] This means that approximately 1 in 3 light duty vehicles in the UK use diesel engines. Furthermore, in 2014, 50% of all new registration vehicles in the UK were diesel, while 48% were petrol and 2% were alternative fuel vehicles. This increase in diesel engines has led to predictions that diesel fuel will be the number one transport fuel in the world by 2020.[7]

Primary vehicle exhaust emissions can exist in the gas phase or as liquids or solids in aerosols, where the partitioning between the phases is determined by the compound's vapour pressure, its occurrence as a pure substance or as a mixture in the condensed phase and its water solubility. Once emitted into the atmosphere the compounds with vapour pressures of $>10^{-5}$ atm, $10^{-5} - 10^{-11}$ atm and $<10^{-11}$ atm, at ambient temperature are expected to be volatile (in the gas phase), semi volatile and non-volatile (in the condensed phase), respectively. A semi-volatile organic compound (SVOC) includes any compound with >1% of its mass in both the condensed and vapour phases.[8] The composition of primary vehicle exhaust aerosol and its contribution to secondary organic aerosol (SOA) formation still remains elusive, where many uncertainties exist relating to the semi-volatile component of the particles.

Diesel exhaust particles consist mainly of agglomerated solid carbonaceous material and ash, together with organic and sulphur containing compounds.[9] The solid carbon is formed during combustion and is subsequently oxidised, while a small fraction of the fuel and motor/lubricating oil are not oxidised and are emitted as VOC/SVOCs in the exhaust. The fraction associated with unburned fuel and lubricating oil is known to vary with engine design and operating conditions, ranging from <10 % to >90 %.[9] Many studies have investigated the composition of the organic

fraction of the particles, reporting targeted groups of compounds such as aliphatic-alkanes, cyclic-alkanes, polycyclic aromatic hydrocarbons (PAH), steranes and hopanes.[10-14] Limited studies, however, focus on higher carbon number species (>C_{15}) owing to instrumental/experimental limitations.[15, 16] The SVOC in diesel exhaust emissions are typically hydrocarbons in the C_{15} – C_{25} range, and are largely uncharacterised because they are unresolved by traditional gas chromatography and form a large hump in the chromatogram referred to as Unresolved Complex Mixture (UCM). To add further complexity, the composition of exhaust aerosol is also dependent upon the sampling collection method. When collecting diesel exhaust aerosol, it is diluted and cooled, which leads to the transformation of gas phase volatile species in the tail pipe into solid and liquid PM.[17, 18] Dilution and cooling processes therefore determine the relative amounts of species that adsorb and/or condense onto existing particles and nucleate to form new particles.[19-21]

The size distribution of diesel PM has been extensively studied.[9, 21-27] The majority of the particle mass exists in the 100 – 300 nm diameter range (accumulation mode) and is where the carbonaceous agglomerates and associated adsorbed materials are found. Approximately 1 – 20% of the particle mass and >90 % of the particle number exists in the 5 – 50 nm diameter range (nucleation mode) and is where the volatile organic and sulphur containing compounds that form during exhaust dilution and cooling are assumed to reside.[9] Particles with diameter >2.5 µm (coarse mode) comprise typically 20-50% of the particle mass in the PM_{10} size range. The physico-chemical properties of particles influence their residence time in the atmosphere, and determine their surface area which governs their availability for atmospheric reactions, optical properties of particles will influence atmospheric visibility and light scattering, and human health effects.

This paper presents the use of thermal desorption coupled to comprehensive two dimensional Gas-Chromatography Time-of-Flight Mass-Spectrometry (TD-GC×GC-ToF-MS) to characterise and quantify the composition of SVOC from diesel exhaust emissions, both in the gas and particulate phases. The composition was also investigated for different particle size fractions using collection by cascade impaction (nano-MOUDI), while particle number size distribution was evaluated by sampling with a DMS500.

2.0 Experimental

2.1 Engine sampling

Experiments were conducted with a light-duty diesel engine; 2.2 L, 4-cylinder in-line compression ignition (CI) engine equipped with a common rail direct injection system, a variable-nozzle-turbine (VNT) turbocharger and a diesel oxidation catalyst (DOC). The open engine control unit (Open-ECU)

DOI: 10.1039/C5FD00185D

allows full control over the engine operating parameters. A schematic of the engine testing system is illustrated in Figure 1.

30 min samples were collected at steady state engine operating conditions at a load of 5.9 bar brake mean effective pressure (BMEP) and speed of 1800 revolutions per minute (RPM), before and after the DOC. Fuel injection pressure was maintained at 1000 bar and a pilot-main fuel injection strategy was used. Exhaust gas recirculation (EGR) percentage was fixed at 12%. Sampling was started after ensuring that the engine was fully warmed-up and thermally stable. Standard European, EN590 specifications, ultra-low sulphur diesel (ULSD, S<10ppm) and 5W-30 part synthetic engine lubricating oil were used for the experiments. Particulate number and size distribution were measured by a Cambustion DMS500 MKII fast particulate analyser and averaged over 1 minute for each sample – 4 samples per experiment. A schematic of the in-house exhaust dilution and sample collection system is shown in Figure 2.

The dilution system incorporates a modified TSI 3302A diluter. The diluter was modified to use cleaned compressed air by using a high flow rate moisture trap and two HEPA filters. The undiluted hot exhaust sample was delivered via a heated line maintained at 191^{o}C and subsequently mixes with the dilution air at ambient temperature. The dilution ratio (DR) was kept at 1:30±5 confirmed by measurements of nitric oxide (NO) before and after the dilution system. The diluted sample was divided into two flow streams, (see Figure 2, labelled 1 and 2). A flow rate of 9 L/min was fixed for stream 1, created by a vacuum pump. A calibrated rotameter and needle valve combination was used to measure the flow rate, and was removed while sampling to avoid particle losses. The second rotameter downstream of the adsorption tube was fixed to ensure the flow rates remained constant throughout the engine sampling period. A nano-Micro Orifice Uniform Deposit Impactor (nanoMOUDI) 125 instrument (MSP Copley Scientific, UK) was utilised for collecting different size particles via this flow stream. The nanoMOUDI has fourteen stages with nominal 50% cut-points of 10,000, 5600, 3200, 1800, 1000, 560, 320, 180, 100, 56, 32, 18, 10 and <10 nm. The sample was collected for 30 min, using polypropylene backed PTFE 47 mm filters (Whatman, Maidstone, UK). Stream 2, demonstrated a fixed flow rate of 1.8 L/min. Stainless steel thermal adsorption tubes packed with 1cm quartz wool, 300mg Carbograph 2TD 40/60 (Markes International) were used to collect gas phase constituents from stream 2; downstream of a polypropylene backed PTFE 47 mm filter (Whatman, Maidstone, UK) to remove any particulates. The temperatures at the sampling points were 25±5^{o}C.

DOI: 10.1039/C5FD00185D

2.3 Analytical instrumentation

Adsorption tubes were desorbed using thermal desorption (Unity 2, Markes International, Llantrisant, UK) and samples were subsequently analysed using a gas chromatograph (GC, 7890A, Agilent Technologies, Wilmington, DE, USA) equipped with a Zoex ZX2 cryogenic modulator (Houston, TX, USA). The first dimension was equipped with a SGE DBX5, non-polar capillary column (30 m, 0.25 mm ID, 0.25 µm – 5% phenyl polysilphenylene-siloxane), and the second dimension column equipped with a SGE DBX50 (4.0 m, 0.1 mm ID, 0.1 µm – 50% phenyl polysilphenylene-siloxane). The GC×GC was interfaced with a Bench-ToF-Select, time-of-flight mass spectrometer (ToF-MS, Markes International, Llantrisant, UK). The scan speed was 50 Hz with a mass range of 35 to 600 *m/z*. Ionisation energies that were explored in this work were 14 eV and 70 eV. All data produced were processed using GC Image v2.3 (Zoex Corporation, Houston, US).

2.2 Analysis of samples

The filters were spiked with 50 µL of 1ng/ µL deuterated internal standards for quantification. Filters were immersed in dichloromethane (DCM), ultrasonicated for 20 min at 20°C. The extract was concentrated to 50 µL under a gentle flow of nitrogen for analysis using GC×GC-ToF-MS. 1 µL of the extracted sample was injected in a split ratio 100:1 at 300°C. The initial temperature of the primary oven (120°C) was held for 2 min and then increased at 2°C/min to 210°C, followed by 1.5°C/min to 325°C. The initial temperature of the secondary oven (120°C) was held for 2 min, and then increased at 3°C/min to 200°C, followed by 2°C/min to 300°C and a final increase of 1°C/min to 330°C to ensure all species passed through the column. The transfer line temperature was 330°C and the ion source temperature was 280°C. Helium was used as the carrier gas at a constant flow rate of 1 mL/min.

Adsorption tubes were desorbed using TD. Briefly, the tubes were spiked with 1ng of deuterated internal standard for quantification, and desorbed onto the cold trap at 350°C for 15 min (trap held at 20°C). The trap was then purged onto the column in a split ratio of 102:1 at 350°C and held for 4 min. The initial temperature of the primary oven (90°C) was held for 2 min and then increased to 2°C/min to 240°C, followed by 3°C/min to 310°C and held for 5 min. The initial temperature of the secondary oven (40°C) was held for 2 min and then increased at 3°C/min to 250°C, followed by an increase of 1.5°C/min to 315°C and held for 5 min. Helium was used as the carrier gas at a constant flow rate of 1 mL/min.

DOI: 10.1039/C5FD00185D

3.0 Results and Discussion

A typical two dimensional separation for diesel fuel and an engine lubricant is shown in Figure 3A and B, respectively. All compounds were separated by volatility in the x-axis (first dimension) and by polarity in the y-axis (second dimension). Peak identification was based on retention indices and mass spectral data from the (National Institute of Standards and Technology) NIST library. The GC×GC conditions for the two contour plots illustrated in Figure 3A and B are outlined in section 2.2, similar to the filters, and are not optimum conditions for separating diesel or motor oil samples. The purpose for this was to get an indication of the positioning of compounds in the contour plots that are present in the filters and adsorption tubes that may come from diesel fuel and/or engine oil. A detailed investigation of the separation of engine oils and diesel fuel using GC×GC-ToF-MS is given elsewhere[28],[29, 30] Figure 3A shows that diesel fuel contains up to C_{20} compounds which are represented in the first portion of the contour plot, whereas engine oil samples are dominated by C_{18} – C_{36} compounds forming a UCM in the latter portion of the contour plot (Figure 3B). The presence of both these UCMs are observed in transient diesel engine exhaust filter samples using the same GC×GC operating conditions (data not shown here) indicating the importance in identifying constituents in diesel and lubricating oils, which are both precursors of engine exhaust emissions. Sutton et al. (2005) isolated individual hydrocarbon fractions from a UCM of biodegraded crude oil and suggested that the entire oil UCM could contain approximately 250,000 unidentified compounds.[31]

Stainless steel thermal adsorption tubes were used to collect gas phase emissions and analysed using TD-GC×GC-ToF-MS. The chromatogram for a 30 min sample collected at steady state engine operating conditions at a load of 5.9 bar BMEP and speed of 1800 RPM, before the DOC is shown in Figure 4. The 3D chromatographic image indicates an abundance of gas phase constituents up to $C_{22,}$ although *n*-alkanes are present up to C_{33} (RT_1 > 60 min, not shown in Figure 4). The chromatogram is very similar to Figure 1A, the diesel fuel, indicating that the majority of the gas phase hydrocarbon engine emission is from the diesel fuel. Recently, Dunmore et al. (2015) showed how diesel related hydrocarbons could dominate gas phase reactive carbon in urban environments.[32] Their study showed that approximately 60 % of the winter primary hydrocarbon hydroxyl radical reactivity was from diesel related hydrocarbons and that they could contribute to up to 50 % of the ozone production potential. The authors measured up to C_{13} and estimated the unmeasured diesel emissions (up to C_{22}) using fuel composition-based emission factors from Gentner et al. (2013).[33]

Approximately 12,000 peaks were found in the chromatography illustrated in Figure 4(A) for the gas phase samples compared to 8000 for the diesel fuel (Figure 1A). Compounds that were identified

include straight and branched alkanes (C_{11} – C_{33}) (Figure 4B), cycloalkanes (C_{11} – C_{25}) (Figure 4C), C9-C12 aromatics (Figure 4D and 4E), naphthalenes (Figure 4F), as well as aldehydes, ketones, alkanoic acids, alkyl benzenes, nitriles, alkyl phenyl ketones, alkyl-biphenyls, furans, furanones, decalins, PAH and sulphur containing compounds including benzothiazole and diphenyl sulfone. Compounds not found in the NIST library were further investigated and tentatively identified using the molecular mass of species found at the same retention times from 14eV ionisation mass spectral data.

In addition to the qualitative data above, preliminary quantitative data for n-alkanes, n-alkylcylohexanes and PAHs were calculated in order to be used as surrogates for modelling evaporation and composition changes of traffic induced ultrafine particles.[34] These quantitative data are shown in Table 1 for total PM (gas phase, particulate and total concentrations) and compared to those data measured after the DOC. The DOC is designed to limit the amount of harmful emissions released to the environment from diesel engines. Its primary functions are the oxidation of CO, unburned hydrocarbons and NO, and can also provide some oxidation of soluble organic fraction (SOF) components to improve soot filter performance.[35] Diesel oxidation catalysts typically reduce emissions of PM by 20 – 40 % or more and gaseous emissions by 50 – 70 %.[36] Table 1 shows the concentration reduction of n-alkanes when measuring these species after the DOC, with a total percentage decrease for C_{11} to C_{33} of 19, 28 and 24 % in the vapour, particulate and the sum of the vapour and particulate phases, respectively. These data, for alkanes, suggest that the efficiency of the DOC for higher molecular weight compounds (HMW, *e.g.* >C_{28}), is less than for lower molecular weight compounds (LMW). The total reduction of the sum of vapour and particulate phases for the HMW (C_{28} – C_{32}) was <10 %. The results are, however, indicative of some re-partitioning of the particulate component into the vapour phase.

The efficiency of reducing the particulate emissions for both n-alkylcyclohexanes and n-alkanes is greater than for the gaseous phase. The n-alkylcyclohexane compounds show a total reduction of 19, 27 and 21 % after the DOC, for the vapour, particulate and the sum of the vapour and particulate phases, respectively. For C_{12} – C_{26} compounds the total (sum of vapour and particulate phase) concentration reductions were 2592 to 2050 ng/m^3. The concentration reductions of individual compounds in the vapour phase are few, whereas all concentrations in the particulate phase are reduced efficiently by >20 % (for LMW compounds, >C_{20}) and to a lesser extent for HMW (>5 % for >C_{21}). Since the DOC is expected predominantly to adsorb and oxidise vapour, the results appear to reflect very active re-partitioning between the particulate and vapour phases.

PAH concentrations illustrate a larger total reduction of 28, 26 and 27 % after the DOC for the vapour, particulate and the sum of the vapour and particulate phases, respectively. This reduction is

more pronounced for the species that are more likely to be in the gas phase (NAP to ANT).[37, 38] The greater reduction of ANT (68%) in comparison to other PAH in the presence of the DOC may explain why roadside concentrations of ANT are generally low in the UK in comparison to some developing countries.[39, 40] For HMW PAH (PYR to B(a)P) the efficiency of the DOC is reduced for the vapour phase but appears efficient for the particulate phase (see Table 1).

A nanoMOUDI 125 instrument (MSP Copley Scientific, UK) was utilised for collecting different size particles. Each of the fourteen stages of the nanoMOUDI with nominal 50% cut-points of 10,000, 5600, 3200, 1800, 1000, 560, 320, 180, 100, 56, 32, 18, 10 and <10 nm, were analysed using GC×GC-ToF-MS. Approximately 1500 peaks were found in the majority of each of the 13 stage two-dimensional chromatograms, using the blob detection technique performed by GC Image v2.3 (Zoex Corporation, Houston, US) software, with a UCM similar to that found in Figure 1B, engine lubricant; consistent with other studies.[41] Compounds identified included straight and branched chain alkanes (C_{12} – C_{33}), cycloalkanes (C_{11} – C_{25}), alkyl benzenes, PAH, decalins, steranes and hopanes. Sulphur containing compounds that were present in the gas phase were not observed in the particulate phase. The concentration distribution of *n*-alkane compounds throughout the nanoMOUDI is shown in Table 2. Interestingly, the largest concentrations were observed in different size fractions according to MW. For example, for LMW compounds (C_{12} – C_{16}) the largest concentrations measured were in the size fraction 1.0 µm in diameter, whereas for HMW compounds (C_{26} – C_{31}) the largest concentrations were observed in the 0.1 µm diameter particle fraction.

The bold numbers in shaded grey are the largest concentrations found for those carbon number species. There is a clear trend for the maximum concentration of the alkanes to be associated with smaller particles as molecular weight increases. This is probably a consequence of the Kelvin effect which increases the equilibrium vapour pressure, and hence volatility of compounds, as particle surface curvature increases with diminishing particle size. Hence the more volatile lower molecular weight compounds are destabilised, with an increased tendency to partition into the vapour phase as particle size decreases. This result is consistent with the theoretical predictions made within the FASTER project and with the results of thermodenuder experiments.[34, 42] Studies have suggested that particles in the 5 – 100 nm diameter range consist mainly of HMW hydrocarbons associated with engine lubricant,[10, 11] which is in broad agreement with the results in this study as the largest concentrations for C_{32} and C_{33} are found in the smaller size ranges (56 nm diameter) compared to other LMW alkanes (see Table 2). Furthermore, roadside aerosol studies using hygroscopic, organic and volatility Tandem Differential Mobility Analyser techniques have shown that particles in the nucleation mode have partly evaporated leaving a 10 nm non-volatile core. [41]

The sum of the total size fractions indicates that the largest concentrations found in the PM are found in the C_{23} – C_{29} region, which also corresponds to the motor oil UCM region shown in Figure 1B. Schauer et al. (1999) reported that the gas phase portion of the UCM consisted of HMW SVOC, which accounted for slightly less than half that of the total carbonyl mass emission rate, while the particle phase portion of the UCM was similar to motor oil when analysed by GC/MS, consistent with the results found in this study.[41] Figure 5 illustrates the gas/particle phase distribution of *n*-alkane concentrations. A bimodal distribution is observed giving rise to a diesel ($<C_{20}$) source and an engine lubricant (C_{21} – C_{27}) source. Elevated concentrations for the LMW alkanes exist in the gas phase, while HMW ($>C_{24}$) are predominantly in the particle phase.

4.0 Conclusion

Thermal desorption coupled to comprehensive two dimensional Gas-Chromatography Time-of-Flight Mass-Spectrometry (TD-GC×GC-ToF-MS) was exploited to characterise and quantify the composition of SVOC from the exhaust emission. Samples were collected from the exhaust of a diesel engine, before and after a diesel oxidation catalyst (DOC). This preliminary dataset shows that the SVOC was observed to contain predominantly straight and branched alkanes (C_{11} – C_{33}), cycloalkanes (C_{11} – C_{25}), various cyclic aromatics, PAH, decalins and alkyl benzenes. Sulphur containing compounds were observed only in the gas phase, as were ketones, aldehydes and naphthalenes. Particle phase compounds identified were similar to those observed in engine lubricants, while vapour phase constituents were similar to those measured in fuels. Sampling after the DOC showed total reductions of 19, 19 and 28 % for gas phase *n*-alkanes, alkyl-cyclohexanes and PAH, respectively; although the DOC illustrated less efficiency for HMW compounds (in the gas phase). With current DOC technology claiming 50 – 70 % reduction in emissions in the gas phase alone, this study shows that there is large variation between compound classes and compounds within a compound class, most probably due to reactivity.

Although studies have reported the size distribution and composition of fine PM emitted from diesel engines, with chemical speciation such as sulphate, ammonium, nitrate, EC and OC;[43-45] or have investigated gas and particle phase tailpipe emissions reporting VOC, SVOC and particle associated OC,[41] very limited studies have investigated the organic composition of diesel exhaust emissions corresponding to different size fractions. We present the *n*-alkane (C_{12} – C_{33}) concentrations measured in 13 different size fractions, showing an increase in the non-volatile concentration with decreasing size fractions. The mode peak for different alkanes was found to be dependent upon

MW, with HMW concentrations peaking at 56 – 100 nm and LMW concentrations peaking at 1 µm. Gas and particle phase distributions of alkanes were also presented showing an overall (total) bimodal distribution, with > 70 % in the gas phase for compounds ≤ C_{20} and < 30 % for compounds ≥ C_{20}. The DOC tested is of very limited efficiency (4 – 68 % for the compounds measured); under the studied engine operating conditions, and appears to cause substantial re-partitioning of compounds from the condensed phase into vapour.

5.0 Acknowledgements

This work is part of the FASTER project, sponsored by the European Research Council (ERC). The authors would also like to thank Yasser Al Qahtani for his contribution during engine sampling.

6.0 References

1. R. M. Harrison, M. Dall'Osto, D. C. S. Beddows, A. J. Thorpe, W. J. Bloss, J. D. Allan, H. Coe, J. R. Dorsey, M. Gallagher, C. Martin, J. Whitehead, P. I. Williams, R. L. Jones, J. M. Langridge, A. K. Benton, S. M. Ball, B. Langford, C. N. Hewitt, B. Davison, D. Martin, K. F. Petersson, S. J. Henshaw, I. R. White, D. E. Shallcross, J. F. Barlow, T. Dunbar, F. Davies, E. Nemitz, G. J. Phillips, C. Helfter, C. F. Di Marco and S. Smith, *Atmospheric Chemistry and Physics*, 2012, **12**, 3065-3114.
2. J. L. Mauderly, *Environmental Health Perspectives*, 1994, **102**, 165-171.
3. M. Masiol, A. Hofer, S. Squizzato, R. Piazza, G. Rampazzo and B. Pavoni, *Atmospheric Environment*, 2012, **60**, 375-382.
4. J. Rissler, E. Swietlicki, A. Bengtsson, C. Boman, J. Pagels, T. Sandström, A. Blomberg and J. Löndahl, *Journal of Aerosol Science*, 2012, **48**, 18-33.
5. P. Pant and R. M. Harrison, *Atmospheric Environment*, 2013, **77**, 78-97.
6. SMMT, *The Society of Motor Manufacturers and Traders - Motor Industry Facts 2015*, 2015.
7. ExxonMobil, *The Outlook for Energy: A view to 2040, Tech. rep., Exxon Mobil Corporation, Texas*, 2014.
8. N. M. Donahue, A. L. Robinson, C. O. Stanier and S. N. Pandis, *Environmental Science & Technology*, 2006, **40**, 2635-2643.
9. D. B. Kittelson, *Journal of Aerosol Science*, 1998, **29**, 575-588.
10. H. Sakurai, H. J. Tobias, K. Park, D. Zarling, K. S. Docherty, D. B. Kittelson, P. H. McMurry and P. J. Ziemann, *Atmospheric Environment*, 2003, **37**, 1199-1210.

11. H. J. Tobias, D. E. Beving, P. J. Ziemann, H. Sakurai, M. Zuk, P. H. McMurry, D. Zarling, R. Waytulonis and D. B. Kittelson, *Environmental Science and Technology*, 2001, **35**, 2233-2243.
12. J. J. Schauer, M. J. Kleeman, G. R. Cass and B. R. T. Simoneit, *Environmental Science and Technology*, 1999, **33**, 1578-1587.
13. B. Zielinska, J. Sagebiel, J. D. McDonald, K. Whitney and D. R. Lawson, *Journal of the Air & Waste Management Association*, 2004, **54**, 1138-1150.
14. L. Huang, S. V. Bohac, S. M. Chernyak and S. A. Batterman, *Atmospheric Environment*, 2015, **102**, 228-238.
15. A. W. H. Chan, G. Isaacman, K. R. Wilson, D. R. Worton, C. R. Ruehl, T. Nah, D. R. Gentner, T. R. Dallmann, T. W. Kirchstetter, R. A. Harley, J. B. Gilman, W. C. Kuster, J. A. de Gouw, J. H. Offenberg, T. E. Kleindienst, Y. H. Lin, C. L. Rubitschun, J. D. Surratt, P. L. Hayes, J. L. Jimenez and A. H. Goldstein, *Journal of Geophysical Research: Atmospheres*, 2013, **118**, 6783-6796.
16. G. Isaacman, K. R. Wilson, A. W. H. Chan, D. R. Worton, J. R. Kimmel, T. Nah, T. Hohaus, M. Gonin, J. H. Kroll, D. R. Worsnop and A. H. Goldstein, *Analytical Chemistry*, 2012, **84**, 2335-2342.
17. B. Giechaskiel, M. Maricq, L. Ntziachristos, C. Dardiotis, X. Wang, H. Axmann, A. Bergmann and W. Schindler, *Journal of Aerosol Science*, 2014, **67**, 48-86.
18. M. Matti Maricq, *Journal of Aerosol Science*, 2007, **38**, 1079-1118.
19. E. M. Lipsky and A. L. Robinson, *Environmental Science and Technology*, 2006, **40**, 155-162.
20. A. L. Robinson, N. M. Donahue, M. K. Shrivastava, E. A. Weitkamp, A. M. Sage, A. P. Grieshop, T. E. Lane, J. R. Pierce and S. N. Pandis, *Science*, 2007, **315**, 1259-1262.
21. I. Abdul-Khalek, D. Kittelson and F. Brear, *SAE Technical Paper*, 1999, **1999-01-1142**.
22. M. J. Kleeman, J. J. Schauer and G. R. Cass, *Environmental Science and Technology*, 2000, **34**, 1132-1142.
23. A. Charron and R. M. Harrison, *Atmospheric Environment*, 2003, **37**, 4109-4119.
24. J. Schneider, N. Hock, S. Weimer and S. Borrmann, *Environmental Science and Technology*, 2005, **39**, 6153-6161.
25. A. Domínguez-Sáez, M. Viana, C. C. Barrios, J. R. Rubio, F. Amato, M. Pujadas and X. Querol, *Environmental Science & Technology*, 2012, **46**, 11187-11194.
26. T. Rönkkö, A. Virtanen, K. Vaaraslahti, J. Keskinen, L. Pirjola and M. Lappi, *Atmospheric Environment*, 2006, **40**, 2893-2901.
27. L. Pirjola, M. Karl, T. Rönkkö and F. Arnold, *Atmos. Chem. Phys.*, 2015, **15**, 10435-10452.
28. M. S. Alam, C. Stark and R. M. Harrison, *Analytical chemistry*, 2015, **Submitted**.

29. G. S. Frysinger and R. B. Gaines, *Journal of High Resolution Chromatography*, 1999, **22**, 251-255.
30. D. R. Gentner, G. Isaacman, D. R. Worton, A. W. H. Chan, T. R. Dallmann, L. Davis, S. Liu, D. A. Day, L. M. Russell, K. R. Wilson, R. Weber, A. Guha, R. A. Harley and A. H. Goldstein, *Proceedings of the National Academy of Sciences*, 2012, **109**, 18318-18323.
31. P. A. Sutton, C. A. Lewis and S. J. Rowland, *Organic Geochemistry*, 2005, **36**, 963-970.
32. R. E. Dunmore, J. R. Hopkins, R. T. Lidster, J. D. Lee, M. J. Evans, A. R. Rickard, A. C. Lewis and J. F. Hamilton, *Atmos. Chem. Phys.*, 2015, **15**, 9983-9996.
33. D. R. Gentner, D. R. Worton, G. Isaacman, L. C. Davis, T. R. Dallmann, E. C. Wood, S. C. Herndon, A. H. Goldstein and R. A. Harley, *Environ Sci Technol*, 2013, **47**, 11837-11848.
34. I. Nikolova, A. R. MacKenzie, X. Cai, M. S. Alam and R. M. Harrison, *Faraday Discussions*, 2015, **Submitted**.
35. A. Russell and W. S. Epling, *Catalysis Reviews*, 2011, **53**, 337-423.
36. T. V. Johnson, *SAE Technical Paper*, 2001, DOI: 10.4271/2001-01-0184.
37. M. S. Alam, J. M. Delgado-Saborit, C. Stark and R. M. Harrison, *Atmospheric Chemistry and Physics*, 2014, **14**, 2467-2477.
38. I. J. Keyte, R. M. Harrison and G. Lammel, *Chem Soc Rev*, 2013, **42**, 9333-9391.
39. M. S. Alam, J. M. Delgado-Saborit, C. Stark and R. M. Harrison, *Atmospheric Environment*, 2013, **77**, 24-35.
40. M. A. Alghamdi, M. S. Alam, J. Yin, C. Stark, E. Jang, R. M. Harrison, M. Shamy, M. I. Khoder and I. I. Shabbaj, *Science of The Total Environment*, 2015, **506–507**, 401-408.
41. J. J. Schauer, M. J. Kleeman, G. R. Cass and B. R. T. Simoneit, *Environmental science & technology*, 1999, **33**, 1578-1587.
42. P. Tiitta, P. Miettinen, P. Vaattovaara, J. Joutsensaari, T. Petäjä, A. Virtanen, T. Raatikainen, P. Aalto, H. Portin, S. Romakkaniemi, H. Kokkola, K. E. J. Lehtinen, M. Kulmala and A. Laaksonen, *Atmospheric Environment*, 2010, **44**, 976-986.
43. M. J. Kleeman, J. J. Schauer and G. R. Cass, *Environmental science & technology*, 2000, **34**, 1132-1142.
44. M. A. Robert, M. J. Kleeman and C. A. Jakober, *Journal of the Air & Waste Management Association*, 2007, **57**, 1429-1438.
45. M. A. Robert, S. VanBergen, M. J. Kleeman and C. A. Jakober, *Journal of the Air & Waste Management Association*, 2007, **57**, 1414-1428.

DOI: 10.1039/C5FD00185D

Tables and Figures

Table 1. Concentrations of n-alkanes, n-alkylcyclohexanes and PAH in the vapour phase, particulate phase and sum of vapour and particulate phase, before and after the DOC, and their percentage reductions

Table 2. Concentrations (ng/m3) of n-alkanes (C12 – C33) in the particulate phase size fractions 10 µm to 0.01 µm measured using nano-MOUDI 125ii. The bold numbers in shaded grey are the largest concentrations found for those carbon number species.

Figure 1. Schematic of the engine testing system

Figure 2. Schematic of the exhaust dilution and sample collection system.

Figure 3. A two dimensional separation (contour plot) of **(A)** diesel fuel, and **(B)** engine lubricant. X-axis separation on a volatility basis; y-axis separation on a polarity basis. Each coloured spot represents an individual species and has a corresponding full mass spectrum. The intense red spots are major peaks, while the blue spots represent less abundant peaks.

Figure 4. 3 dimensional separations of gas phase constituents collected with an adsorption tube and analysed using TD-GC×GC-ToF-MS. **(A)** Total ion chromatogram **(B)-(F)** Selected ion chromatograms. The white solid line signifies 1D chromatography

Figure 5. Gas/particle phase distribution of *n*-alkane concentration

	Vapour phase		% reduction	Particulate phase		% reduction	Total (v+p)		% reduction
	Before DOC	After DOC		Before DOC	After DOC		Before DOC	After DOC	
n-Alkanes (μg/m^3)									
C12	1.07	0.87	18%	0.15	0.05	70%	1.21	0.92	24%
C13	1.07	0.88	18%	0.47	0.30	37%	1.54	1.18	24%
C14	0.90	0.72	20%	0.44	0.28	37%	1.34	1.00	25%
C15	1.00	0.99	1%	0.50	0.27	46%	1.50	1.26	16%
C16	0.62	0.67	-8%	0.51	0.38	24%	1.13	1.05	7%
C17	0.34	0.46	-34%	0.32	0.14	57%	0.67	0.60	11%
C18	0.24	0.20	17%	0.36	0.26	27%	0.59	0.46	23%
C19	0.21	0.16	24%	0.22	0.16	27%	0.44	0.33	25%
C20	0.20	0.10	48%	0.26	0.20	21%	0.46	0.31	33%
C21	0.23	0.05	79%	0.31	0.25	21%	0.54	0.29	45%
C22	0.29	0.06	78%	0.26	0.22	16%	0.55	0.28	49%
C23	0.34	0.07	80%	0.31	0.18	41%	0.65	0.25	62%
C24	0.29	0.09	69%	0.26	0.24	9%	0.56	0.33	40%
C25	0.21	0.08	62%	0.48	0.37	22%	0.68	0.45	34%
C26	0.19	0.10	49%	0.45	0.32	29%	0.64	0.42	35%
C27	0.10	0.11	-8%	0.51	0.28	45%	0.61	0.39	36%
C28	0.10	0.15	-46%	0.49	0.39	21%	0.59	0.54	9%
C29	0.13	0.16	-26%	0.50	0.44	12%	0.63	0.60	4%
C30	0.08	0.14	-72%	0.49	0.41	17%	0.57	0.55	4%
C31	0.10	0.13	-38%	0.42	0.35	17%	0.52	0.48	7%
C32	0.07	0.08	-18%	0.33	0.30	8%	0.39	0.38	4%
C33	0.00	0.00	n/a	0.24	0.19	21%	0.24	0.19	21%
Total	***7.77***	***6.28***	***19%***	***8.28***	***5.97***	***28%***	***16.1***	***12.2***	***24%***
n-Alkyl-cyclohexanes (ng/m^3)									
C12	659.0	540.0	18%	0.0	0.0	n/a	659.0	540.0	18%
C13	295.0	161.0	45%	0.0	0.0	n/a	295.0	161.0	45%
C14	331.0	263.0	21%	33.4	15.1	55%	364.0	279.0	23%
C15	179.0	177.0	1%	61.2	35.6	42%	240.0	212.0	12%
C16	146.0	169.0	-16%	86.7	25.9	70%	233.0	195.0	16%
C17	57.0	49.0	14%	55.0	41.8	24%	112.0	91.0	19%
C18	29.0	35.0	-21%	27.1	12.4	54%	56.0	47.0	16%
C19	12.0	25.0	-108%	63.2	36.0	43%	75.0	61.0	19%
C20	11.0	15.0	-36%	52.1	41.8	20%	63.0	57.0	10%
C21	33.0	17.0	48%	67.7	64.1	5%	101.0	81.0	20%
C22	12.0	13.0	-8%	74.2	69.8	6%	87.0	83.0	5%
C23	37.0	24.0	35%	85.0	82.1	3%	122.0	106.0	13%
C24	14.0	18.0	-29%	58.6	50.0	15%	72.0	68.0	6%
C25	42.0	5.0	88%	49.0	46.1	6%	91.0	51.0	44%
C26	0.0	0.0	n/a	21.3	18.8	12%	21.0	19.0	10%
Total	***1857***	***1511***	***19%***	***734***	***539***	***27%***	***2592***	***2050***	***21%***
PAH (ng/m^3)									
NAP	402.0	281.0	30%	0.0	0.0	n/a	402.0	281.0	30%
ACEY	71.0	47.5	33%	0.0	0.0	n/a	71.0	47.5	33%
ACE	42.7	32.5	24%	0.0	0.0	n/a	42.7	32.5	24%
FLU	38.8	30.6	21%	0.0	0.0	n/a	38.8	30.6	21%
PHE	31.9	19.4	39%	1.5	1.2	23%	33.5	20.6	38%
ANT	38.3	12.2	68%	0.3	0.3	23%	38.6	12.4	68%
PYR	16.1	19.6	-21%	17.9	10.8	40%	34.0	30.4	11%
FLR	18.3	21.5	-17%	18.9	10.8	43%	37.1	32.3	13%
CHR	15.1	15.4	-2%	18.7	13.7	26%	33.7	29.1	14%
B(a)A	11.9	12.0	-1%	13.6	11.1	19%	25.5	23.1	10%
B(a)P	16.6	16.6	0%	8.9	7.5	16%	25.5	24.1	5%
B(ghi)P	0.0	0.0	n/a	30.2	26.5	12%	30.2	26.5	12%
Total	***702***	***508***	***28%***	***110***	***81.8***	***26%***	***812***	***590***	***27%***

Table 1. Concentrations of n-alkanes, n-alkylcyclohexanes and PAH in the vapour phase, particulate phase and sum of the vapour and particulate phase, before and after the DOC, and their percentage reductions

	Size Fractions (μm)														
	<0.010	**0.010**	**0.018**	**0.032**	**0.056**	**0.10**	**0.18**	**0.32**	**0.56**	**1.0**	**1.8**	**3.2**	**5.6**	**10**	**TOTAL**
C number	Concentrations (ng/m^3)														
C12	6.61	6.35	9.04	9.07	12.8	13.4	16.4	18.2	19.6	**20.3**	15.9	16.6	17.0	19.6	201.0
C13	4.15	5.19	7.44	8.28	9.72	7.88	15.7	14.4	19.7	**19.8**	16.5	15.7	16.8	19.6	181.0
C14	5.30	5.41	5.29	7.65	9.46	10.5	12.8	12.6	13.3	**19.4**	15.4	14.0	14.3	18.3	164.0
C15	5.06	5.20	6.55	6.46	6.70	8.13	10.7	12.4	14.8	**21.0**	13.7	11.7	13.9	14.8	151.0
C16	3.66	3.02	3.98	6.42	6.47	7.86	7.84	9.70	10.5	**13.5**	10.4	11.8	12.9	13.3	121.0
C17	4.28	4.54	2.71	4.56	5.74	5.92	8.54	11.0	**14.2**	7.83	10.2	10.6	10.9	12.7	114.0
C18	1.17	1.66	1.27	1.74	2.16	3.07	4.68	5.76	**10.7**	8.23	5.28	3.95	8.23	8.43	66.0
C19	1.89	2.69	2.10	2.69	3.52	3.30	5.64	5.97	**9.90**	8.31	5.30	4.52	5.24	5.21	66.0
C20	2.77	2.20	3.87	4.28	7.74	9.37	12.4	**16.0**	7.54	6.82	4.81	4.24	5.93	5.32	93.0
C21	3.22	2.42	4.96	6.11	9.56	12.0	**20.4**	15.1	9.04	5.60	6.64	6.22	6.18	7.29	115.0
C22	3.47	3.47	8.44	12.4	16.2	18.2	**24.2**	21.3	16.0	16.0	9.98	8.20	4.67	2.40	165.0
C23	8.07	6.33	9.53	15.8	17.9	26.1	**30.2**	26.5	17.7	22.4	18.3	9.16	8.60	2.62	219.0
C24	8.22	6.84	20.1	24.7	30.4	46.8	**53.4**	42.7	37.5	37.7	21.4	18.4	15.1	9.11	372.0
C25	11.1	13.1	28.7	33.4	32.6	45.8	**64.2**	47.1	28.4	42.0	30.9	26.0	9.60	11.2	424.0
C26	12.0	8.96	31.1	24.1	43.6	**53.3**	50.2	41.5	19.8	28.7	22.4	21.8	13.1	10.4	381.0
C27	7.78	8.16	28.9	33.3	46.9	**60.3**	55.8	38.8	17.6	30.0	9.54	17.6	8.44	7.78	371.0
C28	12.0	13.6	26.7	25.3	42.3	**51.6**	46.7	29.2	17.8	19.7	4.67	15.1	5.09	8.44	318.0
C29	16.8	26.8	31.1	44.4	36.2	**47.4**	28.0	22.3	12.0	3.99	3.98	19.1	3.30	2.68	298.0
C30	4.67	2.69	7.13	18.2	21.3	**30.1**	22.4	18.4	17.6	15.8	13.5	11.4	5.18	6.11	195.0
C31	2.77	5.17	6.83	10.2	16.7	**18.9**	16.5	17.5	6.83	6.68	8.35	7.00	3.42	1.70	129.0
C32	7.47	2.60	5.13	12.4	**18.5**	10.3	13.4	13.1	5.13	10.8	8.30	4.97	3.57	4.80	120.0
C33	7.06	8.38	7.79	13.8	**16.8**	11.1	9.47	9.10	7.93	7.62	5.91	4.65	2.94	6.18	119.0
Total	140.0	145.0	259.0	325.0	413.0	501.0	**530.0**	449.0	334.0	372.0	261.0	263.0	194.0	198.0	**4384.0**

Table 2. Concentrations (ng/m^3) of n-alkanes (C12 – C33) in the particulate phase size fractions 10 μm to 0.01 μm measured using nano-MOUDI 125ii. The bold numbers in shaded grey are the largest concentrations found for those carbon number species.

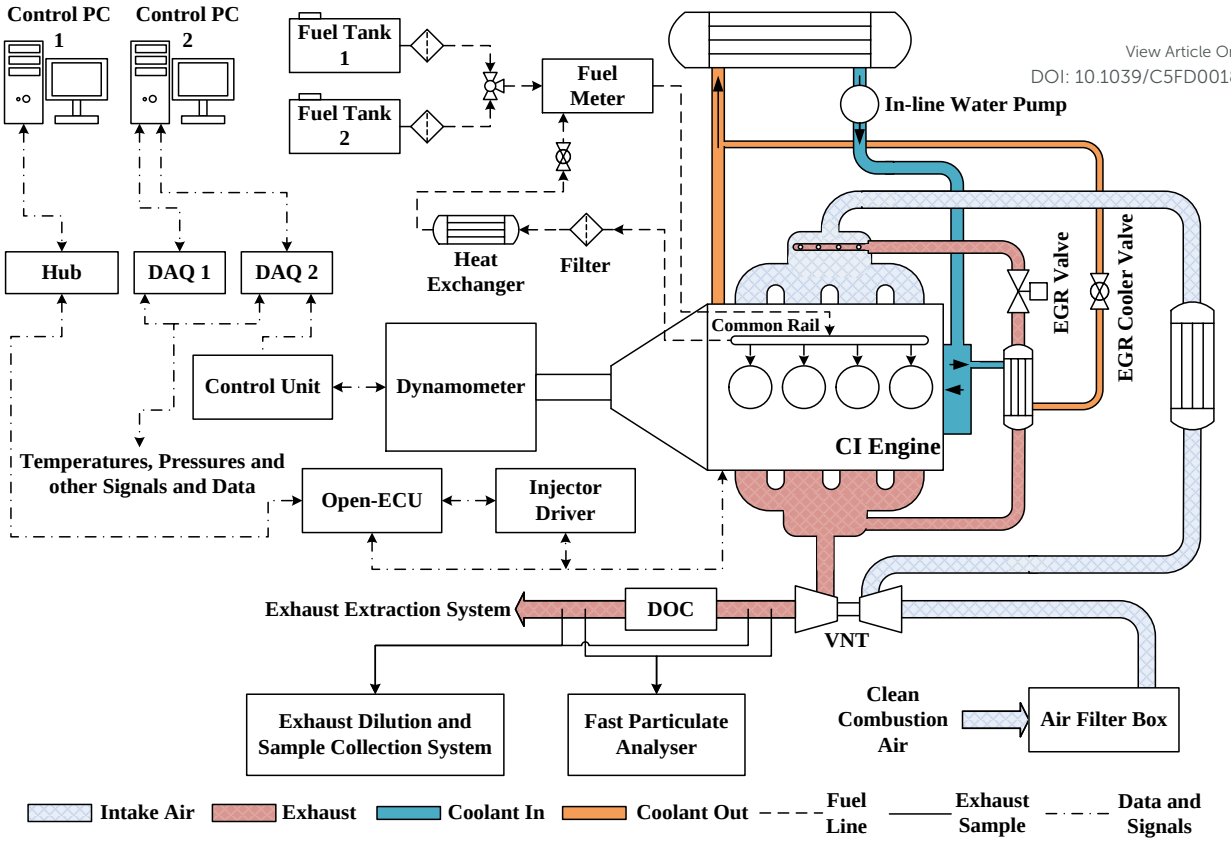

Figure 1. Schematic of the engine testing system

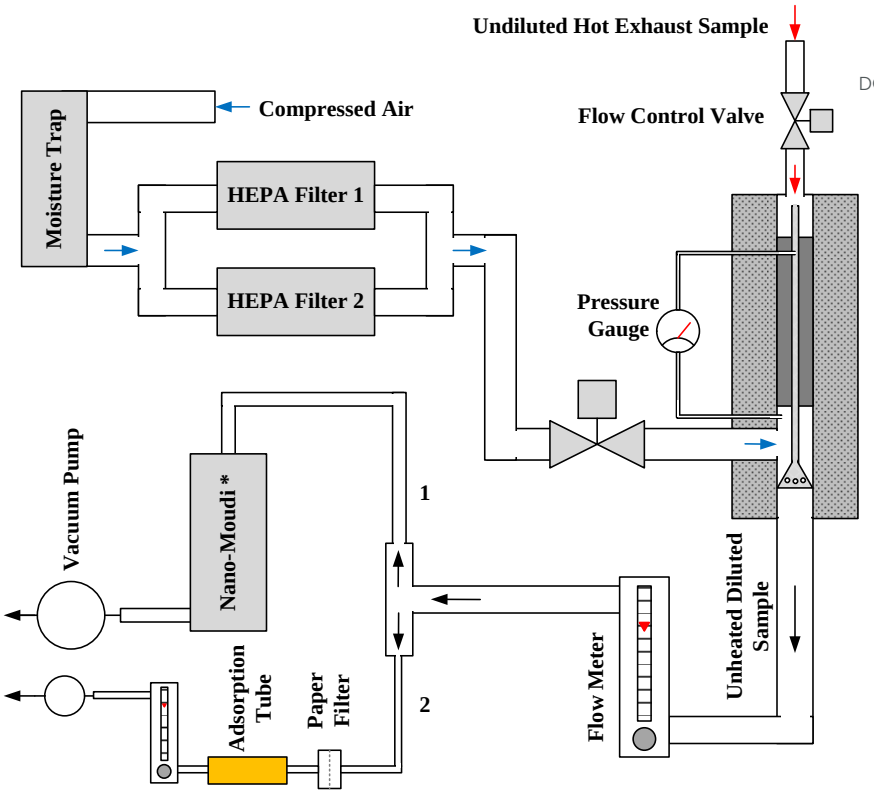

Figure 2. Schematic of the exhaust dilution and sample collection system.

View Article Online
DOI: 10.1039/C5FD00185D

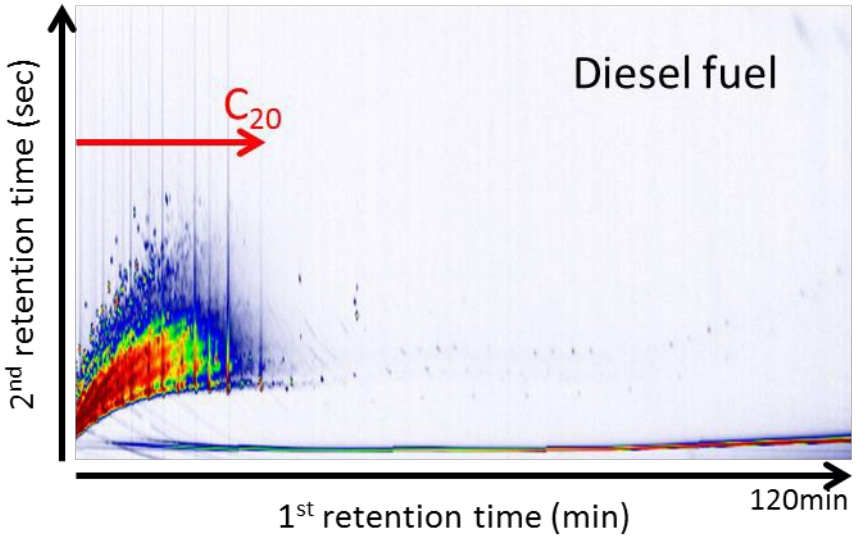

(A)

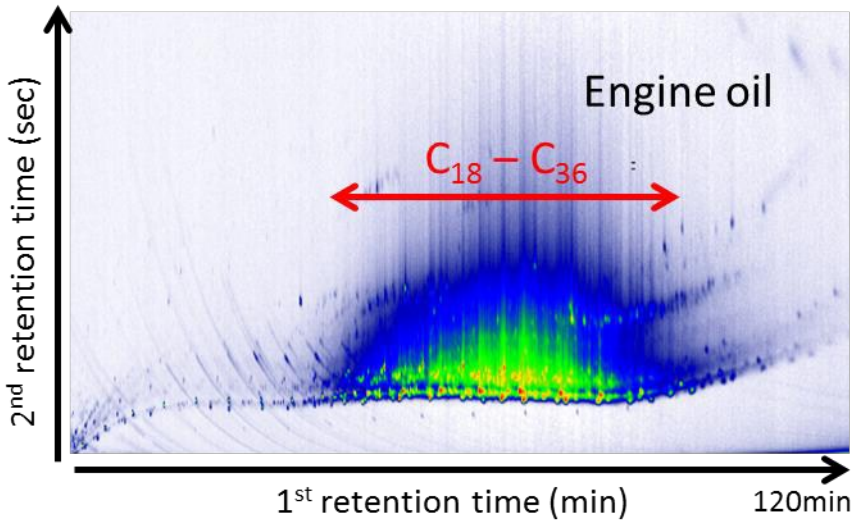

(B)

Figure 3. A two dimensional separation (contour plot) of **(A)** diesel fuel, and **(B)** engine lubricant. X-axis separation on a volatility basis; y-axis separation on a polarity basis. Each coloured spot represents an individual species and has a corresponding full mass spectrum. The intense red spots are major peaks, while the blue spots represent less abundant peaks.

456

457

458

459

460

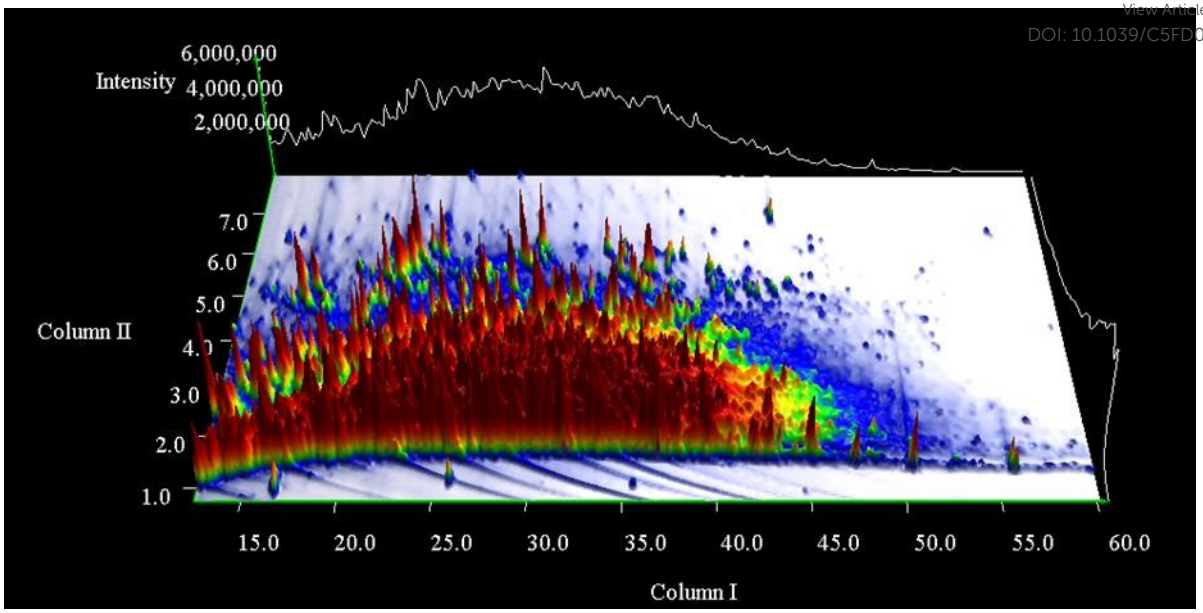

(A) TIC

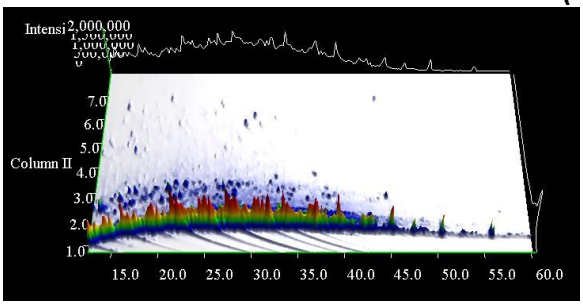

(B) Straight & branched alkanes (m/z = 41, 57, 71)

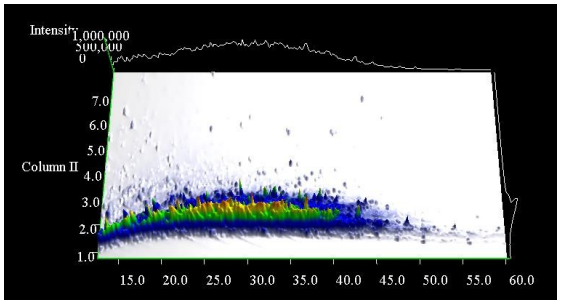

(C) cycloalkanes (m/z = 69, 82, 83, 97, 111)

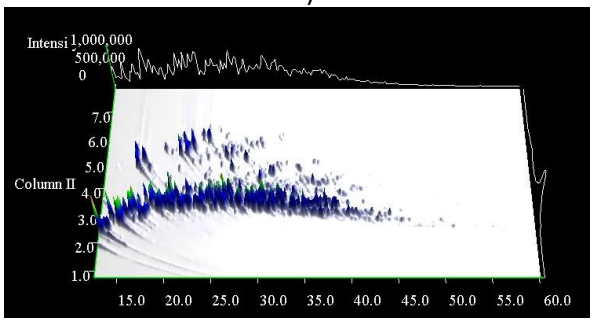

(D) C9 and C10 aromatics (m/z = 105, 119)

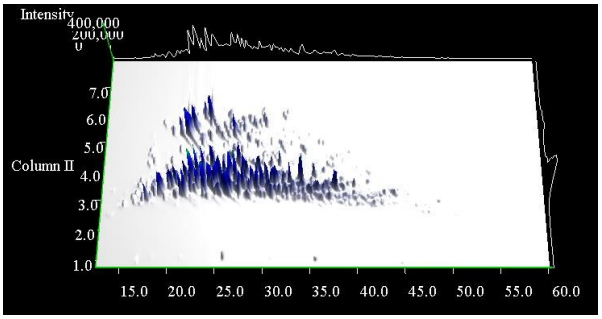

(E) C11 and C12 aromatics (m/z 133, 147)

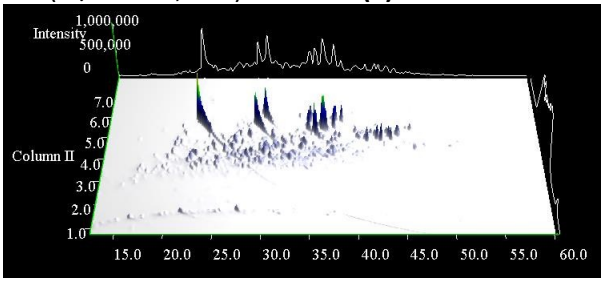

(F) Naphthalenes (m/z = 128, 142, 156, 170, 184)

Figure 4. 3 dimensional separations of gas phase constituents collected with an adsorption tube and analysed using TD-GC×GC-ToF-MS. **(A)** Total ion chromatogram **(B)-(F)** Selected ion chromatograms. The white solid line signifies 1D chromatography.

461

View Article Online
DOI: 10.1039/C5FD00185D

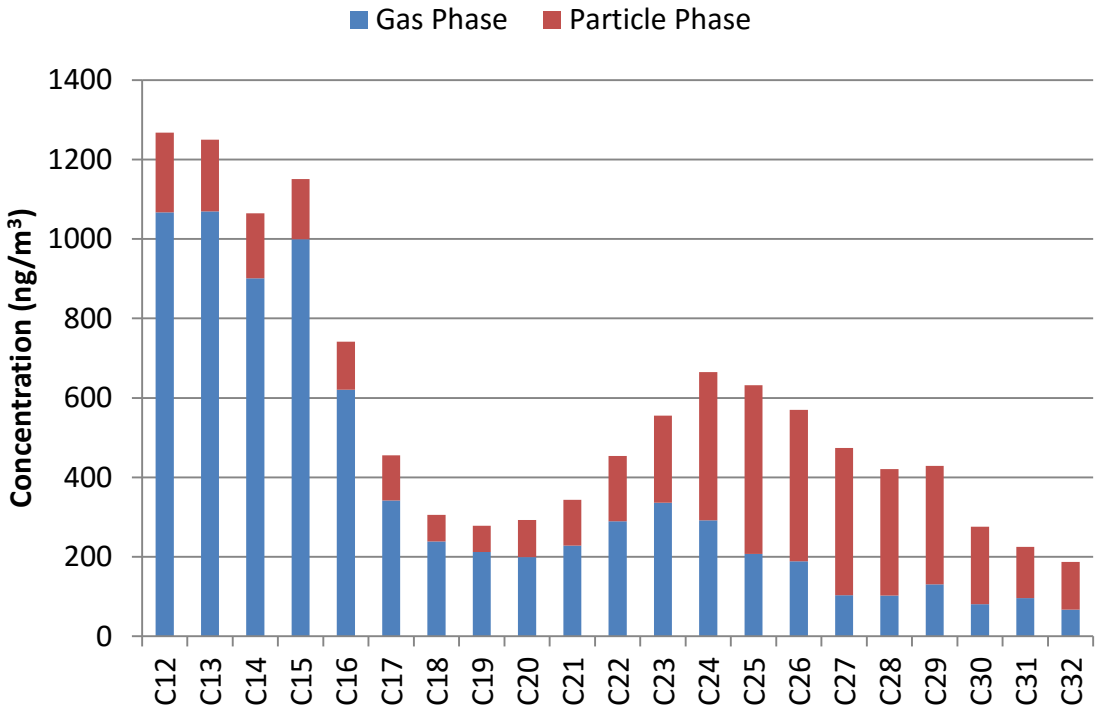

Figure 5. Gas/particle phase distribution of *n*-alkane concentration

462